ELSEVIER

Theoretical and experimental study of electronic temperatures in heavy ion tracks from Auger electron spectra and thermal spike calculations

M. Caron [1], H. Rothard *, M. Toulemonde, B. Gervais, M. Beuve [2]

*Centre Interdisciplinaire de Recherche Ions Lasers, CIRIL-Ganil UMR 6637 (CEA/CNRS/ENSICAEN/Université de Caen),
Boulevard Henri Becquerel, BP 5133, F-14070 CAEN Cedex 05, France*

Abstract

Electron spectra were measured at GANIL with different heavy ions (C–Mo) and various charge states q ($q = 6$–39) at fixed projectile velocity v ($v = 19$ atomic units, 9.2 MeV/u). A projectile dependent broadening of ion induced KVV Auger electron peaks from carbon targets was observed. From this broadening, one can deduce a mean "electronic temperature" of the heavy ion induced track at the corresponding Auger decay time (10 fs). We compare the measured temperature values to the predictions of an inelastic-thermal spike model, which takes into account the electron–phonon coupling. The model underestimates the experimental values, but reproduces the increase with ion charge.
© 2005 Elsevier B.V. All rights reserved.

1. Introduction

The interaction of swift heavy ions with solids may lead to the formation of nuclear tracks in the bulk presenting a cylindrical structure with small diameter (nanometers) but with considerable (macroscopic) length (µm or mm). It thus can be thought of as a quasi-one-dimensional nanostructure [1,2]. The starting point for understanding track formation in solids is the excitation of target electrons and the ejection of electrons along and around the ion trajectory, which finally may be emitted from the solid surface into vacuum [2,3]. Differential electron ejection cross-sections are an important input parameter for numerical simulations of track formation (via "Coulomb explosion" or "thermal spike") in inert matter [2,3], and calculations of the RBE (relative biological effectiveness) of heavy particles in living matter (with important applications in dosimetry and hadrontherapy) [4,5].

Here, we focus on the ejection of carbon KLL Auger electrons induced by swift heavy ions. The experiments were performed with sputter-cleaned amorphous carbon targets in UHV conditions (5×10^{-10} mbar). The spectra were recorded with an electrostatic spectrometer at the medium energy facility SME of GANIL at a fixed observation angle of 140° with 9.2 MeV/u ion beams. The carbon used in these experiments is an electrical conductor. More details on the experiment are given in [6].

Several specific effects connected to the high projectile charge of swift heavy ions in electron emission were observed. Examples are the reduction of low energy electron yields [2,7,8], appearance of hypersatellite lines due

---

* Corresponding author.
 E-mail address: rothard@ganil.fr (H. Rothard).
 [1] Present address: CEA-LEXA, F-51490 Pontfaverger, France.
 [2] Present address: LIRIS and IPNL, Univ. Lyon 1, F-69622 Villeurbanne Cedex, France.

to multiple ionisation of inner shells [2,3,9] and a broadening of Auger lines [10,11]. Examples of electron spectra (and the projectile dependence of the broadening effect) for carbon targets are shown e.g. in [6,10,11]. Also, heavy ion induced electron spectra from other target materials such as Al [12–15], Si [13–15], Be etc. [13] were investigated up to now.

Schiwietz et al. [10] suggested that the broadening of Auger lines could be connected to an increase of the "electronic temperature" of valence electrons. In this paper, we present a comparison of such "electronic temperatures" deduced from a careful analysis of measured heavy ion induced Auger electron spectra to values calculated within the framework of an "inelastic-thermal spike" model.

2. Analysis of electron spectra and deduction of "electronic temperatures"

We have deduced the mean "electronic temperature" of the target for the corresponding Auger decay time (10 fs) by the following procedure as described in more detail in [2,11]. First, we extract the primary Auger spectra, taking into account instrumental resolution and slowing down of Auger electrons during their transport to the surface by means of a numerical simulation [8,11]. The "background" consisting of a continuous ionization electrons and in some cases hypersatellite lines is subtracted [9,11]. The total electron energy distribution $n(\varepsilon, T)$ of the valence electrons results from the convolution of the temperature-dependent Fermi distribution $f(\varepsilon, T)$ and the calculated band structure (density of states) $D(\varepsilon)$: $n(\varepsilon, T) = D(\varepsilon) f(\varepsilon, T)$. We finally adjust the temperature T of the Fermi–Dirac distribution $f(\varepsilon, T)$ so that the total width (not the FWHM) of the calculated electron energy distribution $n(\varepsilon)$ best fits the measured width of the primary Auger spectrum (see [2,11]). No further adjustments of, or assumptions on the primary Auger spectrum are necessary [11].

The energy width of the primary Auger spectra increases as a function of the projectile charge; for example, $\Delta E = 42$ eV with C^{6+} and $\Delta E = 50$ eV with Ni^{27+}. The width of the energy interval of these primary spectra is connected to the energy width of the occupied density of states at the time of the Auger decay. The best fit of the width is obtained at two different temperatures of $T = 11\,600$ K and $T = 24\,000$ K, for C and Ni impact, respectively.

3. The "inelastic-thermal spike" model

In the following description of our "inelastic-thermal spike" model [16], we will lay emphasis on the discussion of the key parameter: the "electron–phonon coupling strength" g in conducting targets. Seitz and Koehler [17] established the theory of the temperature spike. Under the assumption that the electron gas and the atomic lattice are both continuous media, the classical equations of heat flow according to Fick's law can be written as

$$C_e(T_e)\frac{\partial T_e}{\partial t} = \frac{1}{r}\frac{\partial}{\partial r}\left[rK_e(T_e)\frac{\partial T_e}{\partial r}\right] - g(T_e - T_a) + B(r,t) \quad (1)$$

$$C_a(T_a)\frac{\partial T_a}{\partial t} = \frac{1}{r}\frac{\partial}{\partial r}\left[rK_a(T_a)\frac{\partial T_a}{\partial r}\right] + g(T_e - T_a) \quad (2)$$

in cylindrical geometry. C_i, K_i and T_i are the specific heat, the thermal conductivity and the temperature respectively, i is referring either to the electrons (e) or to the lattice atoms (a). g is the coupling constant describing the electron–phonon interaction [18,19] and $B(r,t)$ is the energy deposited in the electron system during the slowing down of the heavy ions (r is the radial distance from the ion trajectory and t the time).

The initial energy deposition time τ is about 0.2×10^{-15} s [20]. In our calculation, we assume a time of 1×10^{-15} s, which corresponds to the slowing down of δ-rays electrons including plasmon de-excitation. We verified that the calculated electronic temperature is nearly independent on the chosen energy deposition time in the interval of 0.2×10^{-15} to 1×10^{-15}. Hence, the evolution of the electronic temperature does not depend strongly on the energy deposition time.

In the present case, we further assume that $B(r,t) = AD(r)\alpha e^{-\alpha t}$ where $\alpha = 1/\tau$ and A is chosen so that the integral of $B(r,t)$ in space and in time gives the value of the electronic stopping power S_e. $D(r)$ is the spatial energy density distribution as deduced from [21] in agreement with Monte Carlo calculations. We note that the importance of the initial energy density distribution was clearly evidenced in yttrium garnet [22,23] for the same value of S_e, lower beam energy results in higher damage cross-section. Such a "velocity effect" was also observed in metals [16,24,25]. Also in the present case, the calculated temperature is rather sensitive to the spatial distribution of deposited energy as can be seen from Fig. 1. The curves 1a and 2a correspond to a beam energy of 1 MeV/u, whereas the curves 1b and 2b correspond to a beam energy of 9 MeV/u. A clear difference between the curves for 1 MeV/u and 9 MeV/u, respectively, is observed. The difference, however, becomes much less pronounced at $\tau = 10$ fs. Note that the initial energy distribution of curve 1a and 2a corresponds to calculations performed by Schiwietz et al. [26] which are more reliable at small radii.

Taking into account the initial spatial energy distribution [21] and the temperature dependence of all the above parameters, the two Eqs. (1) and (2) are solved numerically. The evolution with temperature of the parameters of the electronic subsystem has been described previously [16,25] for crystalline materials and will be applied to estimate the electron–phonon coupling in graphite. The thermodynamic lattice parameters are taken from equilibrium measurements. The only remaining free parameter for crystalline metallic materials is then the electron–phonon coupling strength g [27,28].

Let us now compare experimentally determined g values with a theoretical description of the electron–phonon coupling [27]. If the lattice temperature is not much
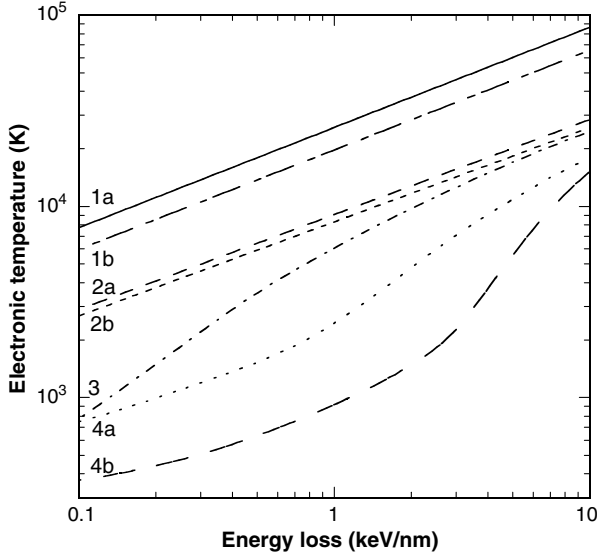
Fig. 1. Calculated electronic temperatures versus energy loss for different combinations of spatial energy deposition, electron–phonon coupling g and electronic diffusivity D_e at 1 fs (maximum temperature) and 10 fs (time of the Auger decay).

(1a) Beam energy of 1 MeV/u, $D_e = 2 \text{ cm}^2/\text{s}$, $g = 0 \text{ W/cm}^3/\text{s}$ at 1 fs,

(1b) beam energy of 9 MeV/u, $D_e = 2 \text{ cm}^2/\text{s}$, $g = 0 \text{ W/cm}^3/\text{s}$ at 1 fs,

(2a) beam energy of 1 MeV/u, $D_e = 2 \text{ cm}^2/\text{s}$, $g = 0 \text{ W/cm}^3/\text{s}$ at 10 fs,

(2b) beam energy of 9 MeV/u, $D_e = 2 \text{ cm}^2/\text{s}$, $g = 0 \text{ W/cm}^3/\text{s}$ at 10 fs,

(3) beam energy of 1 MeV/u, $D_e = 2 \text{ cm}^2/\text{s}$, $g = 3 \times 10^{13} \text{ W/cm}^3/\text{s}$ at 10 fs,

(4a) beam energy of 1 MeV/u, $D_e = 2 \text{ cm}^2/\text{s}$, $g = 1 \times 10^{14} \text{ W/cm}^3/\text{s}$ at 10 fs,

(4b) beam energy of 1 MeV/u, $D_e = 150 \text{ cm}^2/\text{s}$, $g = 1 \times 10^{14} \text{ W/cm}^3/\text{s}$ at 10 fs.

smaller than the Debye temperature T_D, g may be approximated as

$$g = \frac{\pi^2 m_e n_e v^2}{6\tau_e(T_e)T_e} \tag{3}$$

where m_e is the electron mass, n_e the electronic density, $\tau_e(T_e)$ the electron mean free time between two collisions at temperature T_e and v the speed of sound in the metal. v is linked to the Debye temperature T_D and the atomic density n_a by $v = k_B T_D/\hbar(6\pi^2 n_a)^{1/3}$.

The determination of $\tau_e(T_e)$ is very difficult, because no reliable theory is available. To bypass this difficulty, we use the relation of $\tau_e(T_e)$ to the electrical conductivity $\sigma_e(T_e)$ or the thermal conductivity $K_e(T_e)$ of the metal under study so that g reads

$$g = \frac{\pi^4(k_B n_e v)^2}{18 L \sigma_e(T_e)T_e} \quad \text{or} \quad g = \frac{\pi^4(k_B n_e v)^2}{18 K_e(T_e)} \tag{4}$$

where L is the Lorentz number. The evolution of g with temperature follows that of the thermal or electrical conductivity [16]. In the following, g will be determined at 300 K using measured values of the thermal or electrical conductivity of the metal under study. This means that

we assume for g that $K_e(T_e) = K_a(T_a)$ in order to take into account the specific properties of the irradiated material [16]. This is in fact a basic assumption of the model as discussed in [16,25] based on the fact that we rely on measured values of the thermal conductivity as a measure of electron–phonon coupling.

If we assume that the electronic stopping power threshold of defect creation is linked to the appearance of a molten phase [29], we can determine g values for different metals using the inelastic-thermal spike model. In Table 1, we summarise g values deduced from Kaganov's model [27], from the electronic stopping power threshold for damage creation by heavy ions [16] and also from femtosecond (fs) laser experiments [19]. From this table, it is possible to deduce the range of validity of our procedure for the determination of g (assuming one actively participating electron per atom). From fs laser experiments, g values three times lower than predicted are found for Cu, while experiment and calculation are in quite good agreement for Au and Ti. From heavy ion irradiation data (fit of experimental track data to the model), g values are found to be approximately equal to the calculated values for Fe, Bi and C (graphite), but up to five times larger for Ti, Co and Zr. Consequently, it is possible to estimate the g values from Kaganov's theory within better than one order of magnitude as compared to values deduced from experiments.

A direct outcome of Kaganov's theory is that the electron–phonon coupling strength is larger for an amorphous metallic alloy than for the crystalline phase of the same material, since its thermal conductivity is lower [34,35]. This is in agreement with the finding that a material in the amorphous phase is more sensitive to heavy ion irradiation than the same material in its crystalline phase [30,31,36,37]. The g value of crystalline graphite is $3 \times 10^{13} \text{ W/cm}^3/\text{K}$ as deduced by fitting the threshold of damage creation in graphite [33] (Table 1). The known thermodynamical parameters of the lattice [38,39] and the in-plane thermal conductivity (since the irradiation was performed perpendicular to this plane) were used. The calculated g value (Kaganov's theory, Table 1) of $\sim 2.7 \times 10^{13} \text{ W/cm}^3/\text{K}$ (assuming a lattice Debye temperature of 2230 K and one participating electron per atom) is in good agreement with experiment (Table 1). Therefore, $g = 3 \times 10^{13} \text{ W/cm}^3/\text{K}$ is a reasonable estimate for the minimum value of the electron–phonon coupling in amorphous carbon.

Now we have to define the parameters of the electronic subsystem of amorphous materials [37]. Such an adjustment of the parameters has been done by Schiwietz et al. [26] for amorphous carbon. As in the case of crystalline materials, the quasi-free electron gas model will be used. It gives directly the evolution of $C_e(T_e)$ and links $D_e(T_e)$ to the electrical conductivity of the considered material. From experiments, $D_e(T_e)$ at 300 K can be estimated to range between 1 cm²/s and 10 cm²/s. However, it is important to note that the mean diffusion length of the energy on the electrons, $\lambda^2 = D_e(T_e)C_e(T_e)/g$, establishes a link

Table 1
Values of the electron–phonon coupling g (in 10^{10} Wcm^{-3}K^{-1}) for different metals assuming $n_e/n_a = 1$ [25]

Metals (W/cm^3/K)	Kaganov et al. [26] (W/cm^3/K)	fs laser Exp. [19] (W/cm^3/K)	Swift heavy ions (W/cm^3/K)	Calculated threshold (keV/nm)	From experiment (keV/nm)
Cu	13×10^{10}	4.8×10^{10}			
Au	2.3×10^{10}	2.3×10^{10}			
Fe	119×10^{10}		144×10^{10} [16]	~ 45	~ 40 [30]
a-Fe$_{85}$B$_{15}$	2400×10^{10}		500×10^{10} [34,35]	~ 15	~ 13 [31]
Bi	20×10^{10}		13×10^{10} [33]	~ 30	~ 30 [25]
Ti	203×10^{10}	185×10^{10}	1000×10^{10} [16]	~ 12	~ 7 [32]
Graphite	2700×10^{10}		3000×10^{10}	~ 8	~ 7 [33]
Co	90×10^{10}		345×10^{10} [16]	~ 32	~ 35 [32]
Zr	85×10^{10}		260×10^{10} [16]	~ 29	~ 30 [32]

The calculated values from the Kaganov's theory are compared to some experimental values deduced from fs laser experiments [19] or from the fit of track data by the inelastic-thermal spike model ([16], [33], [34,35] and present work for the graphite). The two last columns allow a comparison of the electronic energy loss threshold of damage creation obtained from the calculations and deduced from experiments.

between $D_e(T_e)$ and the electron–phonon coupling strength g. The λ value defines the volume in which the energy is deposited and, consequently, the energy density. In other words, if the electronic energy diffusivity decreases, the electron–phonon coupling should also decrease. Indeed, this has been observed in crystalline materials in order to fit the experimental data [40].

4. Comparison of experimental and theoretical electronic temperatures

The inelastic-thermal spike model as described in the previous section allows to deduce the "electronic temperature" corresponding to the initial deposited energy distribution (T_e^{max}) and at a time of $t = 10$ fs which corresponds to the KVV carbon Auger decay time. The calculations are based on the "metallic" model as described in [25]. The electron density n_e (1×10^{23}) is calculated by assuming one actively contributing valence electron per atom. This is a realistic assumption as shown above.

First of all, we show in Fig. 1 the "maximum electronic temperature" which the system could reach if only the electronic energy deposition at $t \sim 1$ fs is taken into account, as a function of the electronic energy loss dE/dx and for different initial energy depositions, i.e. either the nominal energy deposition of 9 MeV/u and a simulation using 1 MeV/u. No electron–phonon coupling is present ($g = 0$ W/cm^3/s) and the electronic diffusivity is chosen as a reasonable value of $D_e = 2$ cm^2/s [41] close to the minimum possible value of approximately $D_e = 1$ cm^2/s. This value stems from the fact that the mean free diffusion length cannot be smaller than the interatomic distance. Increasing the beam energy from 1 MeV/u to 9 MeV/u decreases the maximum of the electronic temperature by around 25%. In the same conditions, the electronic temperature is given at 10 fs and the difference between the two calculations is less than 10%. In the following we shall take only the calculations performed at 1 MeV/u.

Second, we show in Fig. 1 the calculations for the temperature at the KVV carbon Auger decay time of $t = 10$ fs. Assuming two values of the electron–phonon, the first one

corresponding to graphite ($g = 3 \times 10^{13}$ W/cm^3/s) and second to an estimation of a g value for amorphous carbon ($g = 1 \times 10^{14}$ W/cm^3/s) the use of the electron–phonon coupling decreases the electronic temperature at 10 fs. The effect of a larger initial D_e value leads to the same evolution.

We compare the experimental temperatures for the corresponding Auger decay time (10 fs) from our measurements at 9 MeV/u to the calculations done with a spatial distribution of energy deposition comparable to [26] in Fig. 2. The electronic temperatures are again plotted as a function of the electronic energy loss dE/dx. All of the three different calculations underestimate the experimental values at low dE/dx, although the discrepancy becomes less important at high dE/dx. It is important to note that the most realistic calculation (curve 3), including electron–phonon coupling, underestimates the experimental values by a constant temperature of about 10,000 K. By adding this value to the calculated ones, the model reproduces the increase of the electron temperature with electronic stopping power.
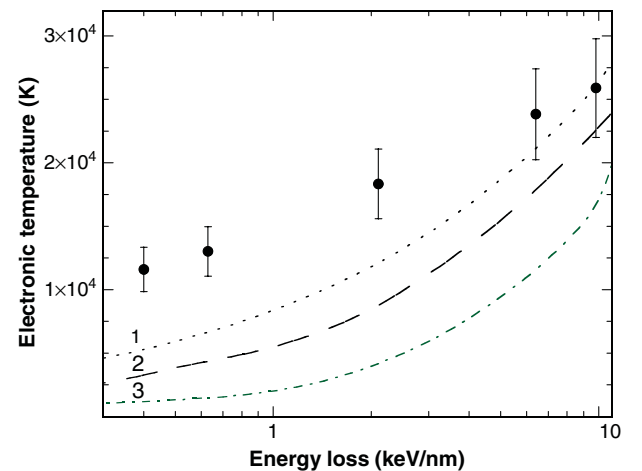

Fig. 2. Comparison of measured (heavy ion induced Auger electron spectra, beam energy of 9 MeV/u) and calculated (inelastic-thermal spike) electronic temperatures.
(1) Beam energy of 1 MeV/u, $D_e = 2$ cm^2/s, $g = 0$ W/cm^3/s at 10 fs,
(2) beam energy of 1 MeV/u, $D_e = 2$ cm^2/s, $g = 3 \times 10^{13}$ W/cm^3/s at 10 fs,
(3) beam energy of 1 MeV/u, $D_e = 2$ cm^2/s, $g = 1 \times 10^{14}$ W/cm^3/s at 10 fs.

Acknowledgements

We thank D. Lelièvre and V. Mouton (CIRIL) for technical assistance. M.C. and M.B. acknowledges Ph.D. grants from CEA and the region of "Basse Normandie". Thanks to G. Schiwietz and K. Czersky for important discussions. The experiment was performed at Ganil/Caen.

References

[1] G. Schiwietz, E. Luderer, P.L. Grande, Appl. Surf. Sci. 182 (2001) 286.

[2] H. Rothard, Nucl. Instr. and Meth. B 225 (2004) 27.

[3] G. Schiwietz, K. Czerski, M. Roth, F. Staufenbiel, P.L. Grande, Nucl. Instr. and Meth. B 226 (2004) 683.

[4] H. Rothard, Radiother. Oncol. 73 (Suppl. 2) (2004) S105.

[5] G. Kraft, Radiobiological effects of highly charged ions, in: F.J. Currell (Ed.), The Physics of Highly and Multiply Charged Ions, Klumer Academic Publisher, 2003.

[6] M. Caron, H. Rothard, M. Jung, V. Mouton, D. Lelièvre, M. Beuve, B. Gervais, Nucl. Instr. and Meth. B 146 (1998) 126.

[7] H. Rothard et al., Nucl. Instr. and Meth. B 125 (1997) 35.

[8] M. Beuve, M. Caron, P.D. Fainstein, M. Galassi, B. Gervais, R.D. Rivarola, H. Rothard, Eur. Phys. J. D 21 (2002) 125.

[9] M. Caron, H. Rothard, M. Beuve, B. Gervais, Phys. Scr. T 80 (1999) 331.

[10] G. Schiwietz, G. Xiao, P.L. Grande, E. Luderer, U. Stettner, Europhys. Lett. 47 (1999) 384.

[11] M. Caron, H. Rothard, M. Beuve, B. Gervais, Phys. Scr. T 92 (2001) 281, more details are given in the thesis of M. Caron (Université de Caen, 2000) which is available from the authors on request.

[12] A. Koyama, O. Benka, Y. Sasa, M. Uda, Phys. Rev. B 34 (1986) 8150.

[13] F. Staufenbiel, G. Schiwietz, K. Czerski, M. Roth, P.L. Grande, Nucl. Instr. and Meth. B 230 (2005) 426.

[14] W. Schmidt, P. Müller, V. Brückner, F. Löffler, G. Saeman-Ischenko, W. Schubert, Phys. Rev. A 24 (1981) 2420.

[15] A. Koyama, H. Ishikawa, K. Maeda, Y. Sasa, O. Benka, M. Uda, Nucl. Instr. and Meth. B 48 (1990) 608.

[16] Z.G. Wang, Ch. Dufour, E. Paumier, M. Toulemonde, J. Phys. Condens. Matter 6 (1994) 6733;
Z.G. Wang, Ch. Dufour, E. Paumier, M. Toulemonde, J. Phys. Condens. Matter 7 (1995) 2525.

[17] F. Seitz, J.S. Koehler, Solid State Phys. 2 (1956) 305.

[18] P.B. Allen, Phys. Rev. Lett. 59 (1987) 1460.

[19] D. Brorson, A. Kazeroonian, J.S. Moodera, D.W. Face, T.K. Cheng, E.P. Ippen, M.S. Dresselhaus, G. Dresselhaus, Phys. Rev. Lett. 64 (1990) 2172.

[20] B. Gervais, S. Bouffard, Nucl. Instr. and Meth. B 88 (1994) 355.

[21] M.P.R. Waligorski, R.N. Hamm, R. Katz, Nucl. Tracks Radiat. Meas. 11 (1986) 309.

[22] A. Meftah, F. Brisard, J.M. Costantini, M. Hage-Ali, J.P. Stoquert, F. Studer, M. Toulemonde, Phys. Rev. B 48 (1993) 920.

[23] A. Meftah, M. Djebara, N. Khalfaoui, M. Toulemonde, Nucl. Instr. and Meth. B 146 (1998) 431.

[24] Z.G. Wang, Ch. Dufour, B. Cabeau, J. Dural, G. Fuchs, E. Paumier, F. Pawlak, M. Toulemonde, Nucl. Instr. and Meth. B 107 (1996) 175.

[25] Ch. Dufour, A. Audouard, F. Beneu, J. Dural, J.P. Girard, A. Hairie, M. Levalois, E. Paumier, M. Toulemonde, J. Phys. Condens. Matter 5 (1993) 4573.

[26] G. Schiwietz, G. Xiao, F. Luderer, P.L. Grande, Nucl. Instr. and Meth. B 164/165 (2000) 353.

[27] I.M. Kaganov, I.M. Lifshitz, L.V. Tanatarov, Zh. Tekh. Fiz. 31 (1956) 273;
I.M. Kaganov, I.M. Lifshitz, L.V. Tanatarov, Sov. Phys. JET 4 (1957) 173.

[28] Ch. Dufour, Z.G. Wang, M. Levalois, P. Marie, E. Paumier, F. Pawlak, M. Toulemonde, Nucl. Instr. and Meth. B 107 (1996) 218.

[29] Z.G. Wang, Ch. Dufour, E. Paumier, M. Toulemonde, Nucl. Instr. and Meth. B 115 (1996) 577.

[30] A. Dunlop, D. Lesueur, P. Legrand, H. Dammak, J. Dural, Nucl. Instr. and Meth. B 90 (1994) 330.

[31] A. Audouard, E. Balanzat, J.C. Jousset, D. Lesueur, L. Thomé, J. Phys. Condens. Matter 5 (1993) 995.

[32] A. Dunlop, D. Lesueur, Radiat. Eff. Defects Solids 126 (1993) 123.

[33] J. Liu, R. Neumann, C. Trautmann, C. Müller, Phys. Rev. B 64 (2001) 184115.

[34] M. Toulemonde, Ch. Dufour, E. Paumier, Phys. Rev. B 46 (1992) 14362.

[35] The calculations performed for amorphous iron boron alloys in [34] have been redone using the model describe in reference [25]. This leads to $g = 5 \times 10^{12}$ W/cm^3/s in order to fit the cross-section of damage creation.

[36] S. Klaumünzer, G. Schumacher, S. Rentzsch, G. Vogl, L. Soldner, H. Bieger, Acta Metall. 38 (1982) 1493;
M.D. Hou, S. Klaumünzer, G. Schumacher, Phys. Rev. B 15 (1990) 1144.

[37] M. Toulemonde, C. Dufour, E. Paumier, F. Pawlak, MRS Proc. 504 (1998) 99.

[38] J. Steinbeck, G. Bruanstein, M.S. Dresselhaus, T. Venkatesan, D.C. Jacobson, J. Appl. Phys. 58 (1985) 4374.

[39] T. Venkatesan, J. Steinbeck, G. Bruanstein, M.S. Dresselhaus, D.C. Jacobson, Phys. Rev. Lett. 53 (1985) 4374.

[40] C. Dufour, F. Beuneu, E. Paumier, M. Toulemonde, Europhys. Lett. 45 (1999) 585.

[41] Yu.V. Martynenko, Yu.N. Yavlinskii, Sov. Phys.-Dokl. 28 (1983) 391.